Collaborative project*

Project acronym: SNM

Project full title: "**Single Nanometer Manufacturing for beyond CMOS devices**"

Grant agreement no: 318804

Deliverable: D11.6 ("Successful demonstration of proof-of-concept of scanning probe alignment adaptable to NIL onto EVG test-setup at TUIL")

Name of the coordinating person: Prof. Dr. Ivo W. Rangelow, Email: ivo.rangelow@tu-ilmenau.de

List of participants:

Participant no.	Participant organisation name	Part. short name	Activity Type	Country
1 (Co)	Technische Universität Ilmenau	**TUIL**	HER	Germany
2	EV Group E. Thallner GmbH	**EVG**	IND; End-user	Austria
3	IMEC	**IMEC**	RES	Belgium
4	Mikrosistemi Ltd	**µS**	SME; End-User	Bulgaria
5	Universität Bayreuth	**UBT**	HER	Germany
6	Technische Universiteit Delft	**TUD**	HER	Netherlands
7	Spanish National Research Council	**CSIC**	RES	Spain
8	IBM Research GmbH	**IBM**	IND; End-user	Switzerland
9	École polytechnique fédérale de Lausanne	**EPFL**	HER	Switzerland
10	SwissLitho AG	**SL**	SME; End-User	Switzerland
11	Oxford Instruments Nanotechnology Tools Ltd	**OINT**	IND; End-user	UK
12	Imperial College London	**IMPERIAL**	HER	UK
13	The Open University	**OU**	HER	UK
14	Oxford Scientific Consultants Ltd	**OSC**	SME	UK
15	VSL Dutch Metrology Institute	**VSL**	IND	Netherlands
16	University of Liverpool	**ULIV**	HER	UK

<table>
<tr><td colspan="11">SNM
Work Package 11
Deliverable: D11.6 (“Successful demonstration of proof-of-concept of scanning probe alignment adaptable to NIL onto EVG test-setup at TUIL”)</td></tr>
<tr><td>Lead beneficiary number</td><td>1</td><td>Nature</td><td colspan="2">R</td><td>Dissemination level</td><td colspan="5">PU</td></tr>
<tr><td>Estimated Person-months</td><td colspan="10">16</td></tr>
<tr><td rowspan="3">Person-months by partner for the Deliverable</td><td>TUIL</td><td>uS</td><td></td><td></td><td></td><td></td><td></td><td></td><td></td><td></td></tr>
<tr><td>16</td><td>2</td><td></td><td></td><td></td><td></td><td></td><td></td><td></td><td></td></tr>
<tr><td colspan="10"></td></tr>
<tr><td>Estimated Delivery Date</td><td colspan="3">M42: 06/2016</td><td colspan="3">Delivery Date</td><td colspan="3">01/09/2016</td></tr>
<tr><td>Author</td><td colspan="10">• Valentyn Ishchuk, Elshad Guliyev, Ivan Buliev, Nikolay Nikolov</td></tr>
<tr><td>Reviewed by:</td><td colspan="10">• WP11 Leader: Thomas Glinsner
• WPG4 Leader: Thomas Glinsner
• Coordinator: Ivo W. Rangelow</td></tr>
<tr><td rowspan="2">Criteria and Achieved Results</td><td colspan="5">Criteria</td><td colspan="5">Achieved result</td></tr>
<tr><td colspan="5">A method and a proof-of-concept for accurately aligning a NIL-Template with a semiconductor wafer capable for positioning accuracy better than 10 nm is being developed.</td><td colspan="5">Achieved. The developed test setup was used for positioning the virtual NIL template and measuring the positioning error of the bottom stage carrying the processed semiconductor wafer with respect to the template holder. The obtained results demonstrate that the bottom stage positioning has proven to achieve the accuracy of sub-10 nm (without temperature drift</td></tr>
</table>

		compensation).
	First measurement tests using the developed proof-of-concept test bench are done.	Achieved. Novel "X"-shaped alignment marks and mini-AFMs were employed for measuring the positioning error of the bottom stage. In this manner, the three degrees of freedom were measured: x, y and φ (rotation around z-axis). The detected offset of the mask was at 8nm (11nm) along x and at 4nm (8nm) along y together with a rotation around its center of 0.60° (3.8° counter) clockwise with resist and without resist cover (in brackets).
Description of the Deliverable	**Motivation and prerequisites** For further downscaling of lithographic features created using Nanoimprint Lithography (NIL) [1] a precise overlay alignment is an essential prerequisite. For example, sub-10 nm lithography for 9 nm node DRAM requires an overlay accuracy of 1.8 nm 3σ [2, 3], which is a challenging technological task. In particular, overlay alignment is a concern for NIL applications using Step & Repeat techniques (SR-NIL), where successive imprints are repeated in order to pattern large areas [4] and an increased number of high accuracy alignment steps are required. More details about the motivation were described in D11.8. The current report presents a proof-of-concept setup which employs a new method for accurately aligning a NIL template with a semiconductor wafer capable for positional accuracy preferably better than 10 nm. Using the implemented test setup, several measurement studies are addressed to test the application of the developed method with respect to the high overlay alignment accuracy. The reported development is based, but not limited to the work described in the following deliverable reports: - The major requirements and basic specification were developed during the initial project period and respectively reported in D11.1 (*"Specification*	

protocol for scanning probe alignment step-and-repeat system");

- Then, the first version of the control electronics was completed and reported in D11.2 (*"SPM multi-channel controller for alignment marks detection"*);
- Various algorithms for image recognition and displacement detection were explored in a simulation environment and the specification was reported in D11.4 (*"Specification: Algorithms for data recognition, displacement detection, automatic overlay alignment"*);
- The system concept was further developed and then, a software package containing supporting functions for automatic overlay alignment during a NIL process was designed; the results were presented in D11.7 (*"Data recognition and alignment software"*).
- The automatic control system was described in D11.8

Motivation for using proof-of-concept test setup

Since the fabrication of a real Nanoimprint Lithography tool (schematically shown in Fig. 11.6.1) is highly expensive and there were not enough available resources for this purpose in the project, it was decided to build a proof-of-concept setup in order to test the developed overlay alignment method, where the overlay alignment procedure is emulated.

The emulation considers a virtual NIL template connected to the two mini-AFMs which are employed for imaging the surface relief marks, i.e. overlay alignment marks. The obtained images are analyzed to position the proof-of-concept setup correctly to align the virtual NIL template. Obviously, we assume a correct calibration of the NIL template to the mini-AFMs. Using such an approach, it is not possible to conclude on a real NIL alignment process since the entire template unit is not integrated into the system. However, the test setup can be used for testing the most crucial point: the positioning of the virtual template in relation to the overlay alignment marks with high accuracy preferably better than 10 nm.

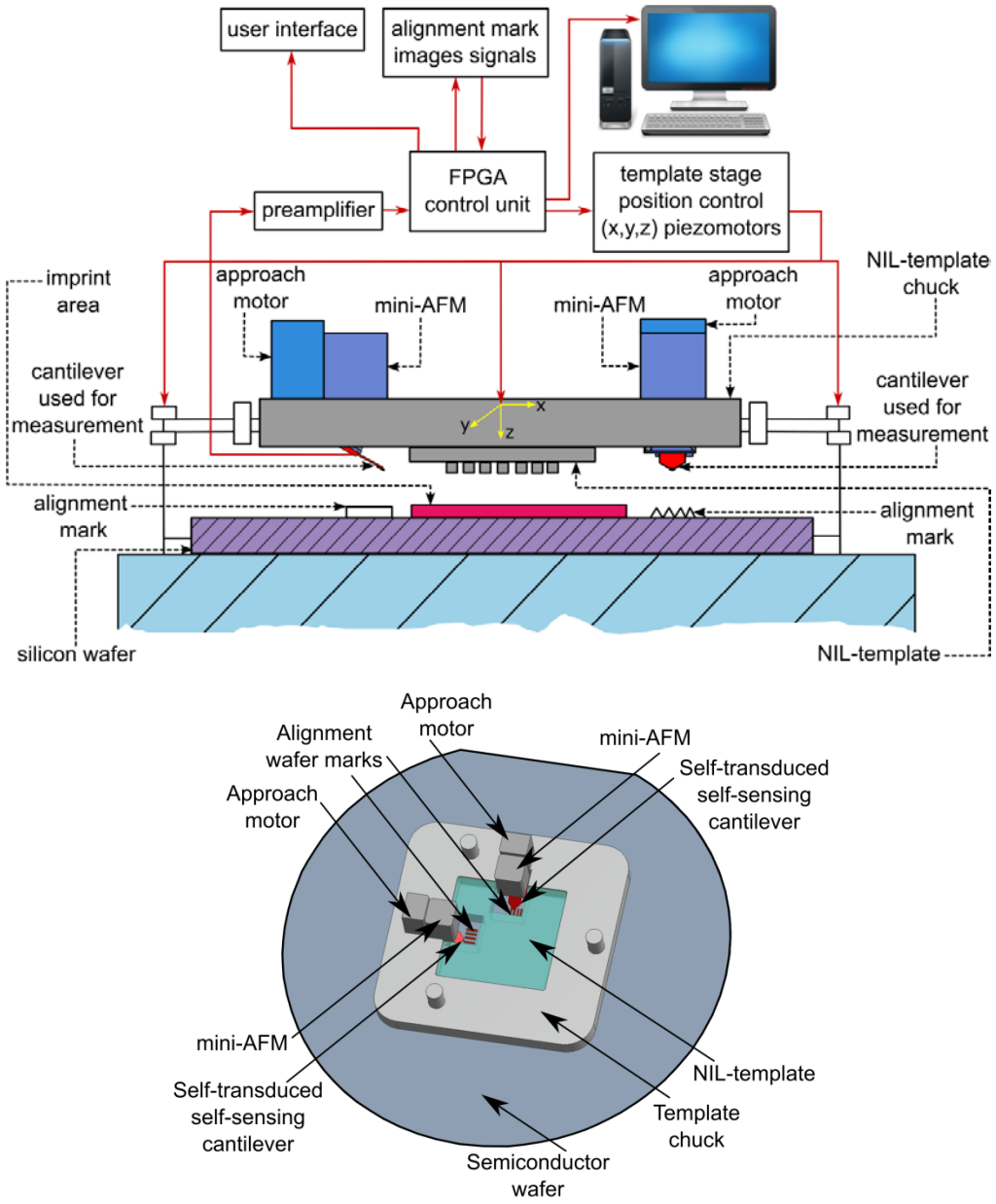

Fig. 11.6. 1 Principle of operation of the NIL setup using the developed alignment method. Frontal and top view of the setup [5].

A detailed description of the system architecture of our envisioned NIL tool (see Fig. 11.6.1) and its components is provided in D11.8. The working principle is described in detail in D11.7.

Proof-of-Concept

Test setup:

The implemented test setup is shown in Fig. 11.6.2 which is used to emulate the alignment procedure.

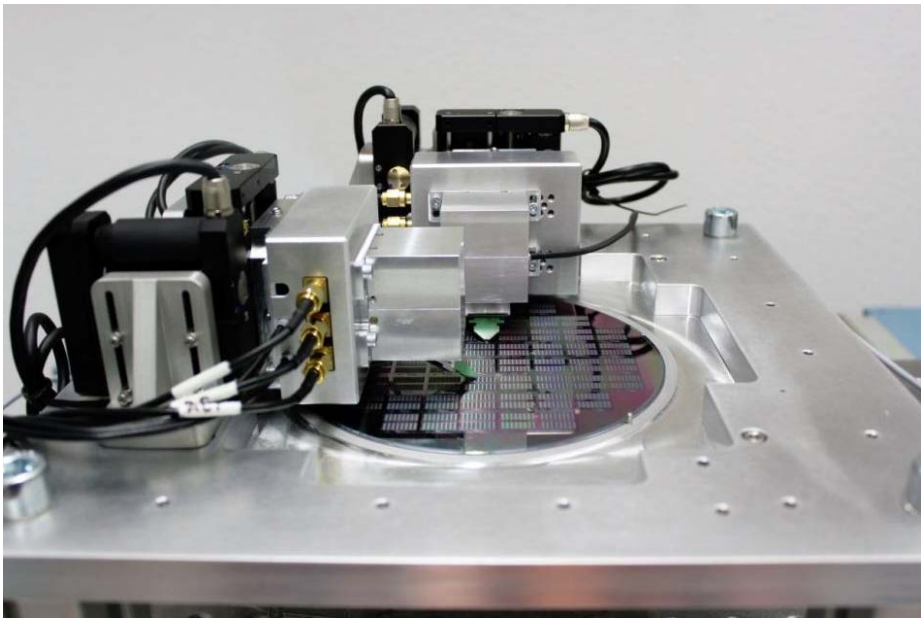

Fig. 11.6.2 Test setup of the alignment Proof-of-Concept (POC)

Hardware: The hardware was described in detail in D11.8 and it comprises all components for a high-speed AFM-system capability: self-sensing, high bandwidth self-actuating cantilever, low noise read-out, high bandwidth z-control employing direct cantilever actuation, fast top-xy-stage [6], and controller for fast data acquisition.

The compactness and ease-of-use of the mini-AFM systems are achieved by using so called active cantilevers [7,8] acting as self-actuating and self-sensing probes [9]. A significant improvement in the performance of such cantilevers with respect to deflection sensitivity and temperature stability has been achieved by using an integrated Wheatstone bridge configuration [10].

Using the described mini-AFMs, alignment marks are detected so that the position of the emulated template to the wafer can be estimated and aligned.

A simple optical setup with 2 µm resolution is used to localize roughly the position of the alignment marks. (It is foreseen that the real tool has miniaturized optical cameras for rough navigation). In the implemented test setup the mini-AFM systems provide the basic tip scanning probe imaging capability of a scan range of 30 x 30 µm with a resolution of 0.1 nm and scan speeds at full scan range of up to 5 lines per second. A fast approach time, e.g. 8 s for 15 mm initial distance ensures a fast processing.

Software: When using the implemented proof-of-concept test setup an overlay alignment procedure is controlled by a computer program. The software package consists of two main parts: a main application including end-user services as calibration of the camera-stage system (described in more detail in D11.8), and detection and alignment to imprint areas and a software library with supporting functions (detailed description is provided in deliverable D11.7).

The main application includes a GUI program module giving the user a possibility to perform manual and semi-automatic detection and calculation of the displacement and rotation. The software library with supporting functions includes a set of procedures for overlay alignment including algorithms for image recognition and displacement identification based on the considered organization of the markers for alignment. These procedures are supposed to serve the main application services, which actually solve calibration tasks, detection of the wafer position and orientation and the imprint itself.

Alignment marks:

The two alignment marks to be scanned have the same design and they have a fixed position with respect to the imprint area and any circuit pattern provided thereon. Accordingly, the mini-AFM cantilever tips have a fixed position relative to the template (template coordinate system), which is measured and known in advance [11]. At the same time, the mini-AFM cantilever tips are accurately aligned with the corresponding alignment marks on the semiconductor wafer [5]. Assuming that the upper frame with the template is correctly positioned with respect to the alignment

marks, the template is accurately aligned with the wafer.

Design of marks: For a reliable overlay alignment, either the edges of the features or the "center of gravity" of the features should be used in terms of the alignment procedure. The "center of gravity" is determined and calculated by the alignment control unit. Detecting the edge of a marker or feature with a high accuracy is repeated more than one hundred times and all measurements are confirming the principle of operation. However, as well known, if we use standard alignment marks comprising only of longitudinal or transversal lines, this can result in difficulties with finding the edges of the features which could be aligned parallel to the scanning direction. For that reason our specially developed X-marks, shown in Fig. 11.6.3, have good capabilities for determining the "center of gravity". The considered "X"-shaped structure was patterned using scanning probe lithography, followed by a subsequent cryogenic etching step [12]. The feature comprises lines of 80 nm width with the average depth of 30 nm. The etching step into silicon was achieved by using SF_6/O_2 plasma in a cryogenic etching system [12].

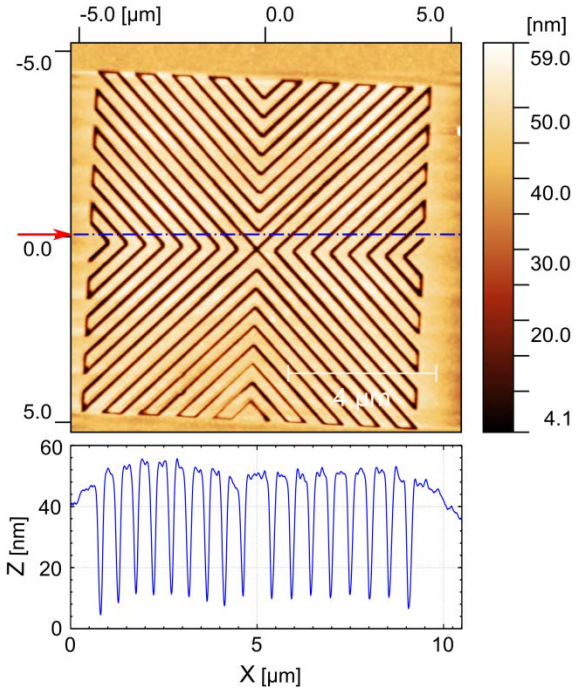

Fig. 11.6. 2 AFM image of "X"-shape alignment mark used in the implemented test procedure. Surface topology profile during AFM-scanning of the utilized "X"-shape alignment mark. Average depth of the patterned lines is 30 nm.

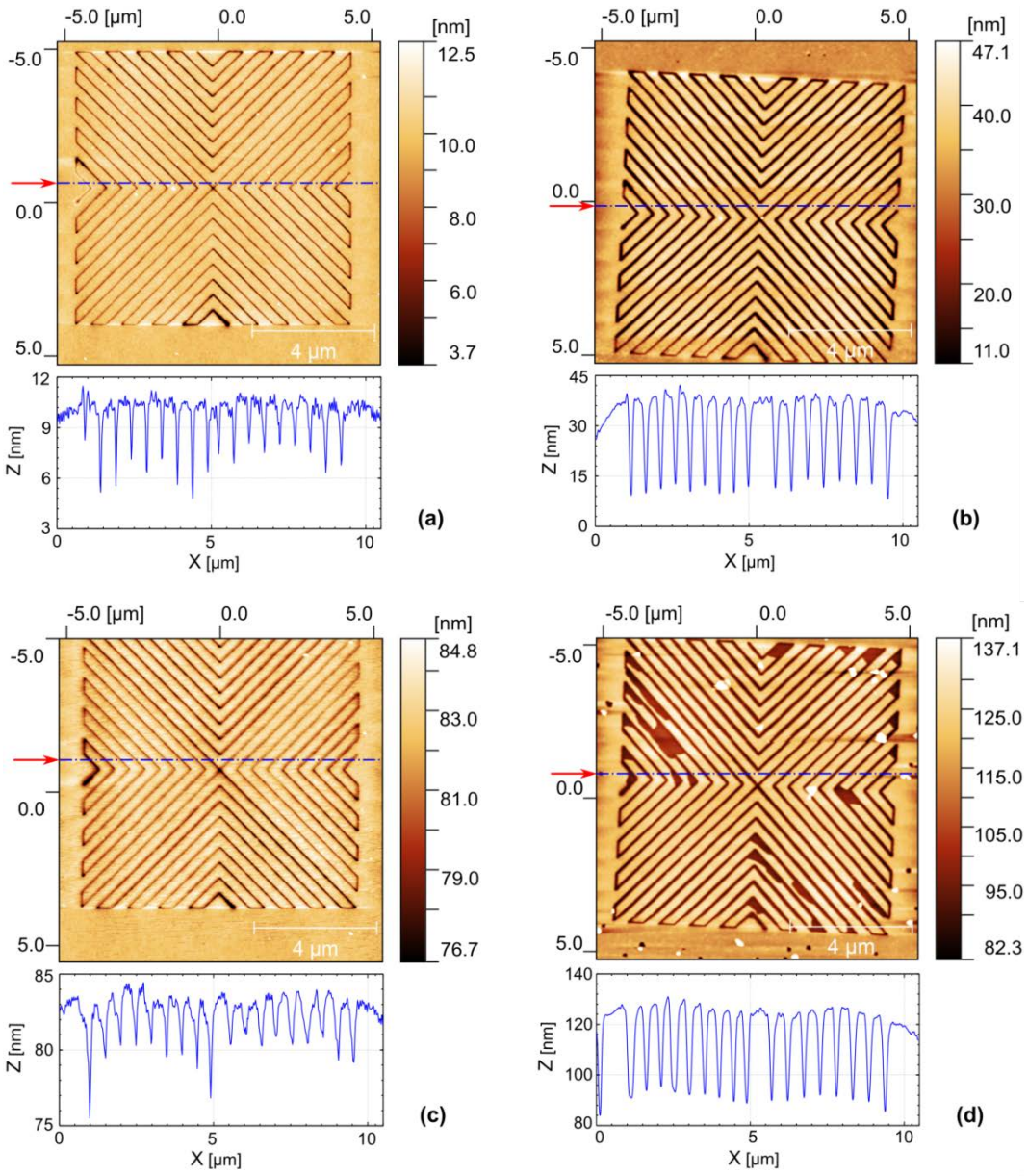

Fig. 11.6. 4. Repeat and reproducibility test. AFM scan and topography profile of two alignment marks at different processing stages. (a): first mark before etching; (b): first mark after etching (good quality of the surface); (c): second mark before etching; (d): second mark after etching (partial damage of the pattern).

Mark detection: The proof of the capability of the mini-AFMs to detect the alignment marks and the mark production was done in two steps. In the first step, the mini-AFM was optically navigated finding the alignment marks shown in Figs. 11.6.4(a) and 11.6.4(c). After that, the wafer was taken out from the setup and etched using cryogenic reactive ion etching process [12, 13, 14]. The wafer was reloaded into the setup and after rough optical navigation the cantilever of the mini-

AFM was employed in order to image the sample surface at the alignment mark position.

The automatic localization and determination of the orientation of the alignment marks is done with the help of cross-correlation type of algorithms [15], while manual localization, and using the metrology tool [11] for validation. The algorithms for automatic localization of the alignment marks rely on a controlled manipulation of an expected image of the region of the mark and comparing it to the actually scanned AFM image of the region. The manipulation is a geometrical transformation with three degrees of freedom – rotation with respect to the center of the image and two translations along the x and y axes of the image. The subsequent comparison has been preliminary implemented in three different ways: (i) as a dot product between vectors of the ordered pixel values of the two images (as in the case of the mathematical correlation function); (ii) as a combination of the normal and inverted versions of the same vectors, thus improving the sensitivity of the detection, and (iii) as a value of a cost function, based on inverting the means square error between the images. In the present work, the first approach has been selected and used taking into account the best results obtained during the testing.
The algorithm requires obtaining a binary bitmap image of the alignment mark area intended for AFM scanning. This can be normally done with the help of a rasterizing tool directly from the vector-graphics design of the layer for transferring. In the present work, this was done manually, using the CorelDRAW as a tool. The bitmap resolution has to correspond to the scanning resolution of the AFM. The size of the bitmap image should be equal to the size of the AFM image if the above mentioned manipulation is performed before the rasterization or bigger if the manipulation is going to be performed on the bitmap image. Expanding the image size in the second case guarantees that a full coverage of the scanned image by the manipulated one can be still achieved. Next, for a given set of a rotation and displacements (φ, x, y), the selected cost function is evaluated. By iterative varying of the values for the angle of rotation and the displacements, a maximum of the cost function is then found. The corresponding set (φ_m, x_m, y_m) is used to describe the relative deviation

of the scanned image from the expected one.

Hence, once the alignment marks have been patterned and precisely measured, their data can be extracted and recognized for different surface coating configurations, which allows a precise alignment of the template at different processing steps of IC manufacturing.

Wafer tilt: For any lithographic application, the issue of wafer tilt is important. For addressing the tilt correction, the following wafer geometry parameters play a considerable role: (i) thickness (ii) total thickness variation (TTV); (iii) warp; (iv) bow. At the moment, the size of the wafer used in the test setup is 150 mm. The size of the template which is accounted for in the presented proof-of-concept is 25 x 25 mm. The wafer used in the experiments was with the total warp below 35 µm and thus for the presented proof-of-concept setup, the impact of the wafer tilt was considered negligible. However, the wafer tilting issue should be taken into account in further experiments, in particular in experiments involving NIL after the final fabrication of the tool in the future.

Recognition of covered marks: Since in the NIL process the pattern will be stamped into a NIL resist layer which covers also the alignment marks, we considered if the mini-AFM is capable to recognize the covered marks. Our experimental tests confirm that even if the patterned alignment mark structure is covered with an additional material layer, e.g. resist, it is still feasible to use it for the alignment procedure (see Fig. 11.6.5). In terms of the experiment, the same structure was scanned twice using

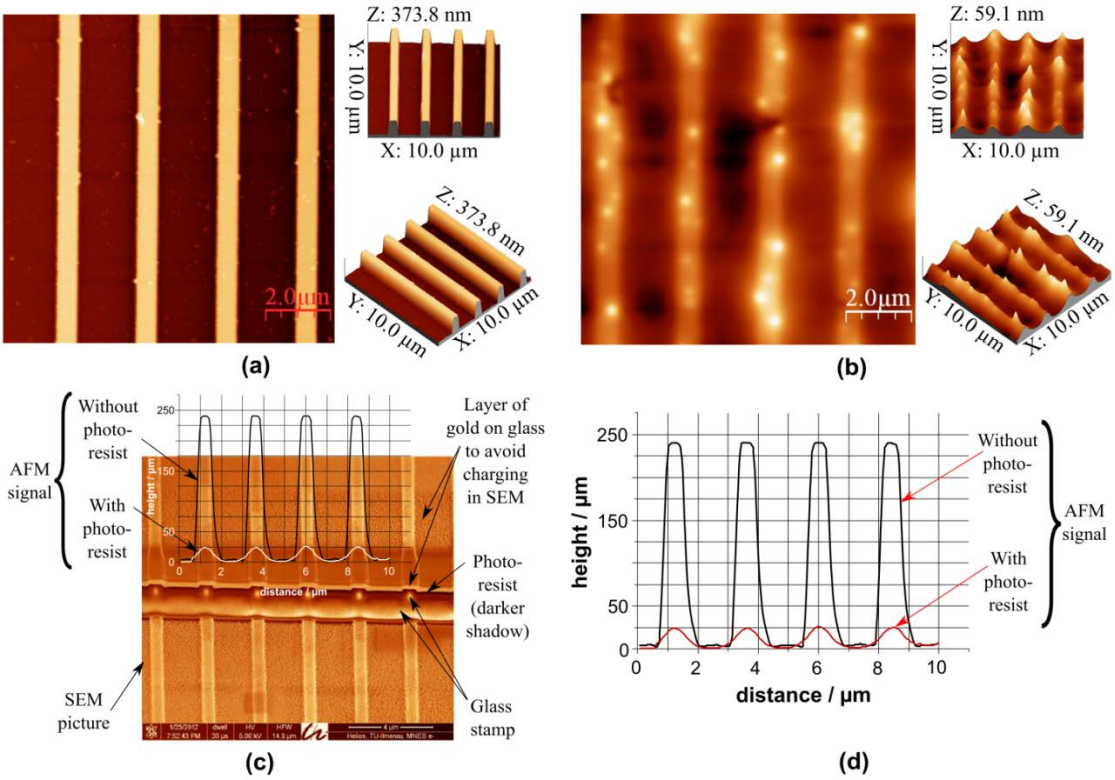

Fig. 11.6. 5 Using mini-AFM for scanning surfaces with the same pattern at different wafer processing stages; (a): the scanned surface without resist; (b): the scanned surface with resist; (c): SEM picture of the considered pattern overlapped with the corresponding AFM topology scan signals; (d): AFM topology scan signals for the surface with / without resist.

AFM, a bare surface without any coverage (Fig. 11.6.5 (a)) and with spin-coated resist layer on top (Fig. 11.6.5 (b)). The profiles of the appropriate surface topology AFM signals shown in Fig. 11.6.5 (c) and Fig. 11.6.5 (d) demonstrate perfect overlapping with respect to the offset – the maxima of the curves with and without resist are off to each other. To detect the real position of alignment marks under the resist (Fig. 11.6.5(d)), the method presented by Rawlings *et al*. [15] can be employed. This method assumes that the final topography profile z could be obtained from the initial topography p by convoluting p with an impulse response function f [15]:

$$z = p * f \tag{1}$$

Using the AFM image of the spin-coated sample the relative position of the alignment marks without resist can be reconstructed. Here, an absolute measurement of the position of the structure edges is not essential; the shape of the signal can itself be used to determine the relative alignment mark position.

Assuming the argument of the function f leads to the central limit theorem, a Gaussian distribution can be selected for f where f is isotropic and thus the σ values are set to be equal for the x and y directions, so that [15]:

$$f(x,y) = \frac{R}{{\sigma_b}^2 2\pi} \exp\left(-\frac{x^2+y^2}{2{\sigma_b}^2}\right), \quad 0 < R < 1. \tag{2}$$

The variables σ_b and R represent respectively the "blurring" and the flattening effect of the considered function f. Since the parameters σ_b and R depend on the spin-coating process conditions (spin speed, solvent, etc.), they must be obtained experimentally [15].

Test the proof-of-concept:

Our proof-of-concept consists of the positioning of the sample with respect to the virtual NIL template, i.e. to the mini-AFMs, and the analysis of the positioning error which is related to the specifications of the wafer carrying bottom stage. The setup allows optical navigation to the alignment mark position. After that, the mini-AFMs analyze the marks and the control-unit (together with the software module) is used to calculate all offsets which are displayed and could be transmitted to the high precision mechanical alignment x, y, φ motors (the x, y - scanning orthogonality of the mini-AFMs is precisely measured with the help of a metrology tool (Nanopositioning and Nanomeasuring Machine from SIOS GmbH, Ilmenau) [11].

The bottom positioning stage is used for steering the sample to compensate the overlay error. The alignment accuracy of the presented system depends on the movement step of the stage. The currently used bottom positioning stage has a movement resolution of 10 nm. Once the displacement error has been determined by the system software, it needs to be compensated by the appropriate stage movement. To achieve this, the movement is done separately for x and y axis in iterative manner, wherein each new step uses the positioning error from the previous step and compensates it adequately. The procedure finishes when the offset between the considered pattern (represented by alignment marks) and the

virtual NIL template (represented by mini-AFMs) is equal or less 10 nm.

The result from an automatic localization of an alignment mark is illustrated in Fig. 11.6.6. The AFM was positioned over the mark and the region was scanned (Fig. 11.6.6(a)). The size of the scanning field was 10 ×10 μm and the image size in pixels – 1024 ×1024. The expected view of the mark is generated and shown in Fig. 11.6.6(b), while the superposition of the two images is in Fig. 11.6.6(c).

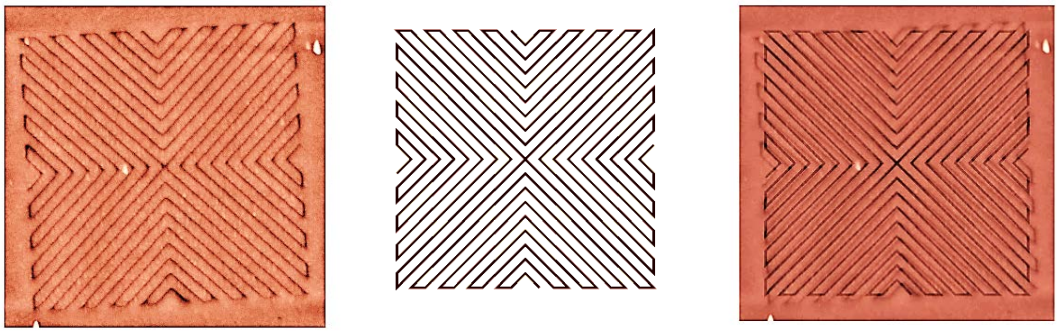

(a) (b) (c)

Fig. 11.6. 6 Scanned image of the alignment mark (a), its expected view (b), and the previous two superimposed to show the displacement (c).

The cross-correlation cost function values were computed for a range of ±25pix displacements along each axis and a set of rotation angles of up to 4 deg with 0.1 deg resolution. The cost function values were stored in a 3D array and then analyzed to find the maximum value. Fig. 11.6.7(a) shows the 2D cost function image for a rotation angle of $3.3°$ where the global maximum was found. The maximum location is at the intersection of the solid lines in the picture, while the dashed lines intersect at the point where the maximum was expected. Based on the current image resolution, the deviation of the scanned mark consists of a displacement along x at one pixel on left, i.e. at -9.8 nm, displacement along y at one pixel down, i.e. at -9.8 nm and a rotation counter clockwise at 3.3°. Using the corresponding set $(3.3°, -9.8\ , -9.8\ )$, the expected image was modified and superimposed over the scanned one. The result clearly proves the sub-10nm overlay alignment capability and is shown in Fig.11.6.7(b).

Similar automatic localization was performed on a zoomed region of the alignment mark (1.5 ×1.5um in 512 ×512 pixels). The corresponding images are presented in Fig. 11.6.8(a-e).

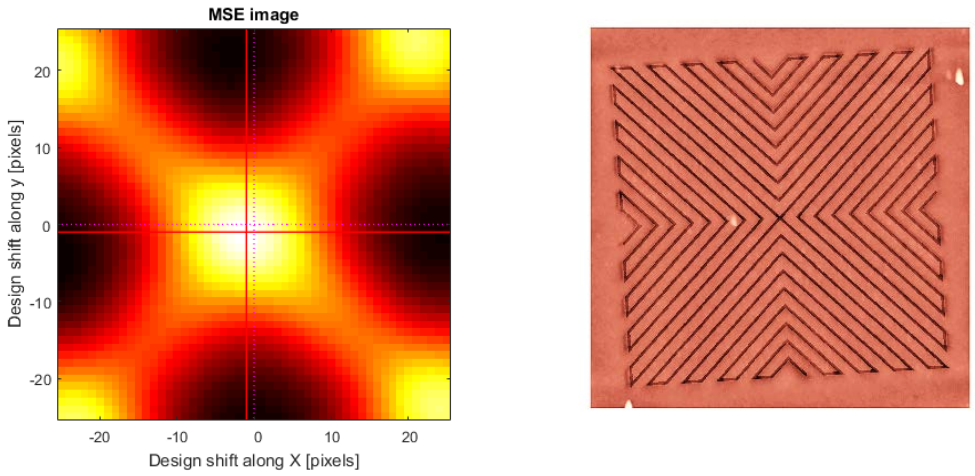

(a) (b)

Fig. 11.6. 7 A 2D slice of the cost function space at 3.3° rotation, with the location of its maximum (a) and the superposition of the scanned image and the corrected expected view of the alignment mark (b).

(a) (b) (c)

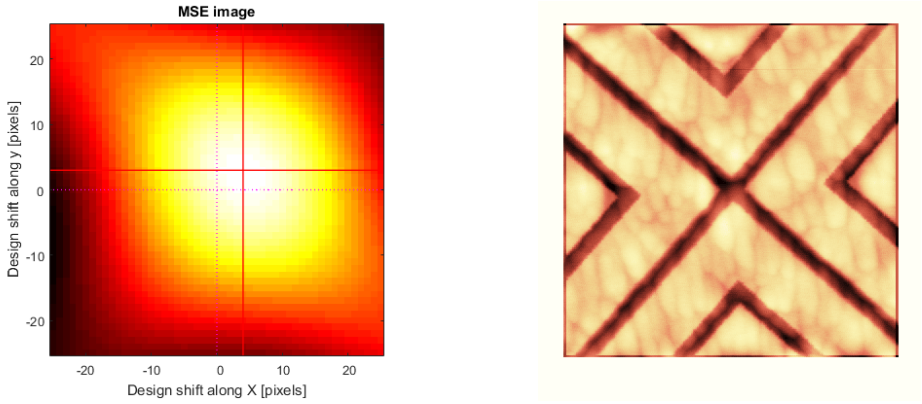

(d) (e)

Fig. 11.6. 8 Scanned image of the alignment mark (a), its expected view (b), the previous two superimposed to show the displacement (c), 2D slice of the cost function space at 3.8° rotation (d), and the superposition of the scanned image and the corrected expected view of the alignment mark (e).

The detected offset of the mask is at +4 pixels along x and at +3 pixels along y, which corresponds to a metric displacement at (+11 nm, +8 nm) together with a rotation around its center at 3.8° counter clockwise.

This is shown in Fig. 11.6.9 were there is also the comparison with and without resist cover on top of the alignment marks. The best result with resist is an X offset of 8nm, an Y offset of 4nm and a rotation of 0.6°. Both results clearly prove the capability of the overlay alignment method for a NIL imprint tool.

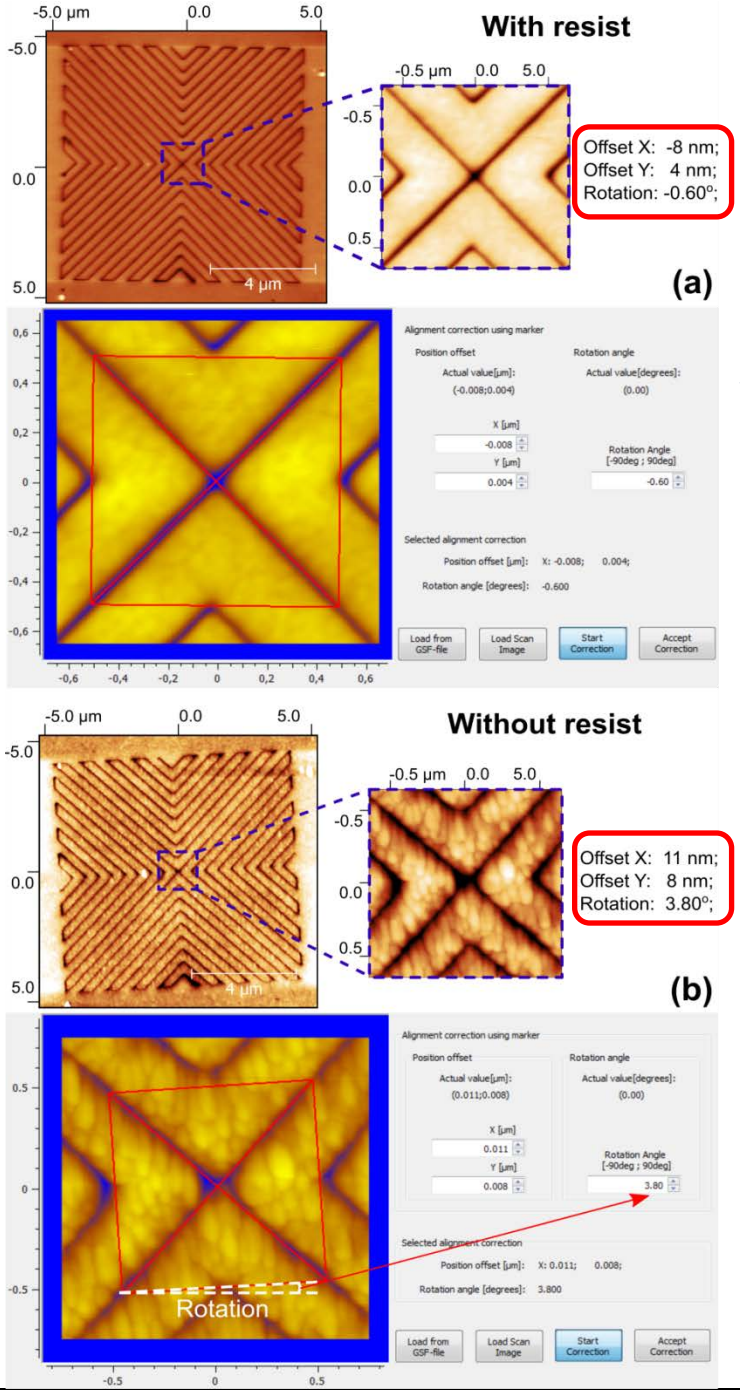

Fig. 11.6. 9 Alignment marks fabricated with Scanning Probe Lithography [16] are used in the tests of the proof-of-concept setup. The surface relief marking utilizes an "X"-shape to allow for obtaining better feature edge contrast. The screenshots from the software illustrate intermediate data in terms of the offset detection.

Summary	In this work, a proof-of-concept setup for emulation of the developed overlay alignment technique for NIL was built and tested. The emulation considers a virtual NIL template represented by two mini-AFMs which are employed for imaging the surface relief marks and thereafter the obtained images are analyzed to determine the offset between the considered pattern and the virtual NIL template. The used mini-AFMs are based on so called active cantilevers, which allow realization of extremely robust and compact AFM-heads. The active piezoresistive probes are comparable to passive probes using optical read-out and allows for easier system integration and significant reduction in the AFM-head weight. In the conducted tests, the developed method was used for positioning the virtual template and measuring the offset between the considered patterns (represented by alignment marks) on the processed semiconductor wafer and the virtual NIL template (represented by mini-AFMs). The obtained AFM images are used to calculate the deviation and steer the bottom stage carrying the wafer to achieve the desired offset accuracy. It was shown that the detection of the offset error can be implemented using “X”-shaped marks and two measurement units (mini-AFMs). In this manner, the three degrees of freedom are measured: x, y and φ (rotation around z-axis). A cross-correlation method was used to determine all position parameters. The obtained results successfully demonstrate the proof-of-concept of the considered scanning probe alignment method.
Explanation of Differences between Estimation and Realization	n.a.

Metrology comments	The proof of concept was performed using mini-AFM scan systems with a resolution down to 0.1nm. There are however additional sources of errors which contribute to the total measurement error: • Line edge roughness, • The thermal drift of the top-frame with the two mini-AFMs, • The accuracy of the pre-patterned alignment marks, • The measurement accuracy of the position of the mini-AFM tips, • The roughness of the spin-coated resist, and • Total electronic noise. Extended analysis of the above errors is a matter of the future work.
References	[1] H. M. Saavedra, T. J. Mullen, P. Zhang, D. C. Dewey, S. A. Claridge, P. S. Weiss, Rep. Prog. Phys. 73 036501 (40pp) (2010) [2] "International technology roadmap for semiconductors 2011 edition", Tables "Lithography 2011", Lithography Technology Requirements, see http://www.itrs2.net/2011-itrs.html, 2016 [3] M. Neisser, F. Goodwin, L. He, "ITRS Roadmapping Process for Lithography", Presentation, February 2013, see http://ieuvi.org/TWG/Mask/2013/MTG022413/13__ITRS_Roadmapping_Process__Frank_Goodwin.pdf, 2016 [4] C. Peroz, S. Dhuey, M. Volger, Y. Wu, D. Olynick, S. Cabrini, Nanotechnology 21, 445301 (2010) [5] I.W. Rangelow, European patent No. EP 1 617 293 A1 (18 January 2006) [6] E. Guliyev, B.E. Volland, Y. Sarov, Tzv. Ivanov, M. Klukowski, E. Manske, I.W. Rangelow, Meas. Sci. Technol. 23 074012 (2012) [7] I.W. Rangelow, P. Skocki, P. Dumania, Microelectron. Eng. 23, 365-368 (1994). [DOI: 10.1016/0167-9317(94)90174-0] [8] R. Pedrak, Tzv. Ivanov, K. Ivanova, T. Gotszalk, N. Abedinov, I.W. Rangelow, K. Edinger, E. Tomerov, T. Schenkel, P. Hudek, J. Vac. Sci. Technol. B 21, 3012 (2003). [DOI: 10.1116/1.1614252] [9] M. Kaestner, T. Ivanov, A. Schuh, A. Ahmad, T. Angelov, Y. Krivoshapkina, M.

Budden, M. Hofer, S. Lenk, J.-P. Zoellner, I.W. Rangelow, A. Reum, E. Guliyev, M. Holz, N. Nikolov, J. Vac. Sci. Technol. B 32, 06F101 (2014)

[10] A. Ahmad, T. Ivanov, T. Angelov, I. W. Rangelow, J. Micro/Nanolith. MEMS MOEMS 14(3), 031209 (2015)

[11] N. Vorbringer-Doroshovets, F. Balzer, R. Fuessl, E. Manske, M. Kaestner, A. Schuh, J.-P. Zoellner, M. Hofer, E. Guliyev, A. Ahmad, T. Ivanov, I. W. Rangelow., Proc. SPIE 8680, 868018 (2013)

[12] V. Ishchuk, D. L. Olynick, Z. Liu, I.W. Rangelow, J. Appl. Phys. 118, 053302 (2015)

[13] I.W. Rangelow, J. Vac. Sci. Technol. A 21, 1550 (2003)

[14] I.W. Rangelow, Surf. Coat. Technol. 97, 140–150 (1997)

[15] C. Rawlings, U. Duerig, J. Hedrick, A.W. Knoll, IEEE Transactions on Nanotechnology 13(6) (2014)

[16] M. Kaestner, C. Aydogan, Tzv. Ivanov, A. Ahmad, T. Angelov, A. Reum, V. Ishchuk, Y. Krivoshapkina, M. Hofer, S. Lenk, I. Atanasov, M. Holz, I.W. Rangelow, J. Micro/Nanolith. MEMS MOEMS 14(3), 031202 (2015)